Reports

Seismic-Wave Attenuation Associated with Crustal Faults in the New Madrid Seismic Zone

R. M. HAMILTON AND W. D. MOONEY

The attenuation of upper crustal seismic waves that are refracted with a velocity of about 6 kilometers per second varies greatly among profiles in the area of the New Madrid seismic zone in the central Mississippi Valley. The waves that have the strongest attenuation pass through the seismic trend along the axis of the Reelfoot rift in the area of the Blytheville arch. Defocusing of the waves in a low-velocity zone and/or seismic scattering and absorption could cause the attenuation; these effects are most likely associated with the highly deformed rocks along the arch. Consequently, strong seismic-wave attenuation may be a useful criterion for identifying seismogenic fault zones.

UNDERSTANDING THE CAUSES OF intraplate seismicity is one of the major problems in earthquake hazard assessment, particularly in the United States. Intraplate seismicity is commonly attributed to zones of crustal weakness, that is, fault zones that are favorably oriented for reactivation in the regional tectonic stress field (*1*). Numerous fault zones are commonly present in intraplate areas; only a few, however, are seismically active. What distinguishes these seismogenic fault zones from the others? To help answer this question, we reanalyzed data from a seismic-refraction survey of the New Madrid seismic zone (NMSZ), in the central Mississippi Valley, where a series of large intraplate earthquakes occurred in 1811 and 1812 (*2*), to search for signs of anomalous seismic-wave propagation.

The NMSZ is located in the upper Mississippi embayment, which is a broad, south-plunging syncline underlain by the Reelfoot rift (Fig. 1) (*3*); aeromagnetic data show that the rift is a northeast-trending graben that is 70 km wide and 300 km long (*4–6*). The rift was probably formed during the late Proterozoic and has been reactivated repeatedly (*7, 8*). A major tectonic episode near the end of the Paleozoic resulted in the formation of the Blytheville arch (also known as Charlie's ridge) (*9–13*) (Fig. 2), possibly contemporaneously with the formation of the Pascola arch (*14*). Rift reactivation during the Mesozoic led to embayment subsidence and pluton emplacement along the rift margins and axis (*6*).

As much as 1 km of unconsolidated Cenozoic and Upper Cretaceous sedimentary rocks fill the Mississippi embayment. The underlying Paleozoic rocks include Upper Cambrian and Lower Ordovician carbonate rocks that are equivalents of the Knox-Arbuckle Megagroup, Upper Cambrian shales of the Elvins Group, Upper Cambrian dolomitic rocks of the Bonneterre Formation, and a thick sequence of Upper Cambrian (?) clastic rocks. The Blytheville arch is defined by strong subhorizontal seismic reflections outside the arch that are warped upward at the arch margin (Fig. 2); under the arch, reflections are virtually absent (*11–13*), which, together with seismicity, suggests that a major fault zone is present. The arch formed when a former basin was uplifted on high-angle faults (*8*).

Earthquake focal depths in the NMSZ are shallow (most are less than 15 km) (*15, 16*), and most of the epicenters occur in several linear trends (Fig. 1) that show the locations of active faults (*17*). The longest zone of seismicity generally coincides with the Blytheville arch along the axis of the rift; earthquake focal mechanisms indicate right-lateral, strike-slip displacement (*18*). The earthquake (inferred body-wave magnitude m_b = 7.2) on 16 December 1811 (*2*) probably was located near the Blytheville arch. The current seismicity is most intense between Dyersburg and New Madrid in the area of the Pascola arch, where earthquake focal mechanisms generally indicate reverse slip on northwest-striking planes (*18–20*). The earthquake on 7 February 1812 (m_b = 7.4), and perhaps the one on 23 January 1812 (m_b = 7.1), may have been located near the Dyersburg–New Madrid seismicity trend (*2*).

In 1980, an extensive seismic-refraction survey was conducted in the NMSZ. Crustal

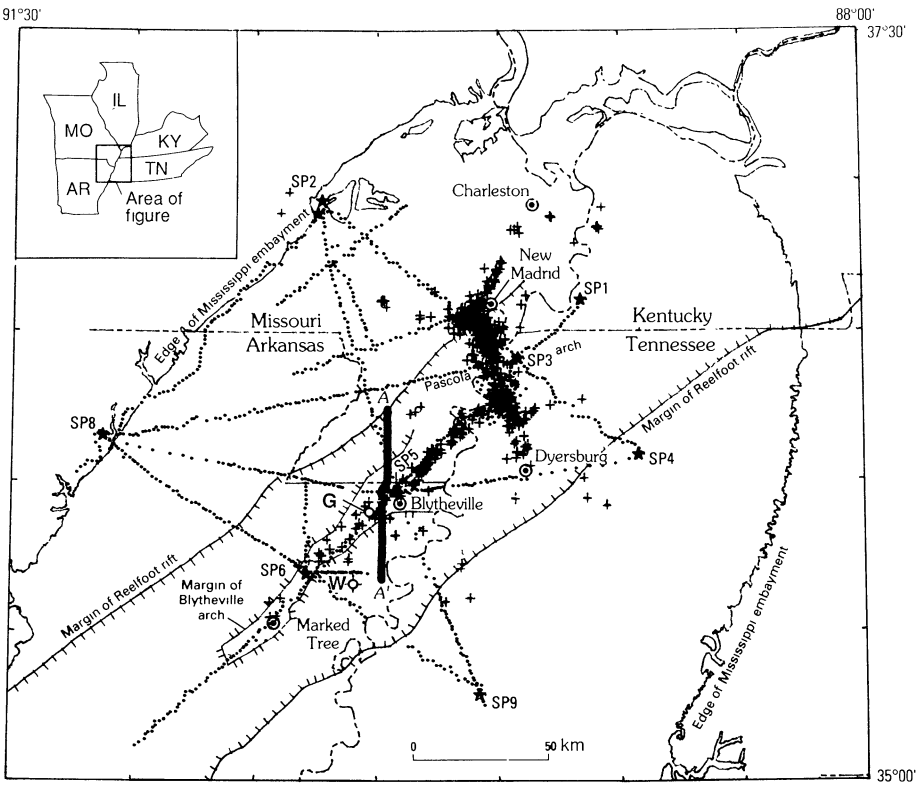

Fig. 1. Map of the New Madrid region showing locations of the seismic-refraction shot points (stars), recording sites (dots), seismic-reflection profile (A–A'), Blytheville arch (*13*), Reelfoot rift (*6*), epicenters (pluses) (*15*), and Dow Chemical #1 Wilson (W) and #1 Garrigan (G) drill holes.

R. M. Hamilton, U.S. Geological Survey, 922 National Center, Reston, VA 22092.
W. D. Mooney, U.S. Geological Survey, 345 Middlefield Road, Menlo Park, CA 94025.

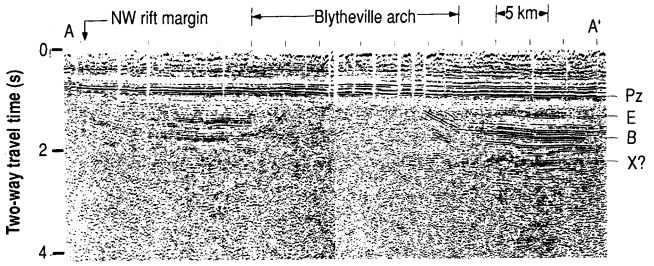

Fig. 2. Seismic-reflection profile across the Reelfoot rift and the Blytheville arch. Profile location A–A′ is shown in Fig. 1. Reflection correlations with stratigraphic horizons are labeled as follows: Pz, top of Paleozoic rocks; E, top of the Elvins shale and base of carbonate rocks; B, Bonneterre dolomite and basal clastics; and X, crystalline basement. The depth of reflections (in kilometers) is about three times the travel time in seconds below Pz plus the amount of time above Pz.

models derived from the refraction data (*21, 22*) have seismic-wave velocities of 1.8 km/s for unconsolidated sedimentary rocks that fill the embayment, 5.95 km/s for carbonate rocks under the embayment fill, 6.2 km/s for crystalline rocks of the upper crust, 6.6 km/s for rocks in the lower crust, and 7.3 km/s for a "pillow" of modified lower crustal rocks under the embayment. An important feature of these models is the presence of a 4.9-km/s low-velocity layer beneath the carbonate rocks, which is interpreted to extend about 40 km in both directions away from the axis of the rift; the presence of this layer was inferred from the rapid attenuation of the 5.95-km/s waves at distances of greater than 25 km. The Blytheville arch introduces a substantial vertical velocity discontinuity in the upper crust that should affect seismic-wave propagation.

In the 1980 seismic-refraction experiment, 34 explosions at nine shot points (SP) and 100 portable seismographs deployed in ten arrays were used (Fig. 1); most of the refraction lines were more than 100 km long. The waves refracted at the boundary between Upper Cretaceous rocks [primary (*P*)-wave velocity of about 1.8 km/s] and the underlying Paleozoic rocks (*P*-wave velocity of about 6 km/s) are most useful for identifying seismic-wave properties in the upper crust. We focused on variations in the amplitude of these refracted first arrivals among the profiles, particularly those in the distance range of 3 to 20 km. We present data for two stations, SP6 and SP5, where variations in attenuation were the greatest.

SP6 is centered over the Blytheville arch, midway along its mapped extent (Fig. 1). Three shots at SP6 were recorded along six arrays extending out from the shot point (Fig. 3). Among all profiles obtained from all shots, the southeast-northwest profiles for SP6 (Fig. 4A) best exhibit a contrast in seismic-wave attenuation; to the southeast, first arrivals are strong to about 12 km and are visible to about 20 km, whereas, to the northwest, they attenuate rapidly beyond 4 km and are barely discernible at 10 km. Arrivals are strong to the northeast (Fig. 4B) and strong to the southwest, are fairly strong to the east (Fig. 4C), and are weak again to the north (Fig. 4D). The profiles that have weak arrivals, the north and northwest azimuths, cross the northwest flank of the Blytheville arch; the profiles that have strong arrivals either follow the southeast flank of the arch or extend east of the arch (Fig. 3). Most seismicity has occurred northwest of the northeast-southwest profiles and, in the vicinity of SP6, toward the northwest side of the arch. This correlation suggests that strong attenuation may be associated with an active fault zone along the northwest margin of the arch.

SP5 is located in the northeast part of the arch (Fig. 1). Two shots at SP5 were recorded on four profiles (Fig. 3). Strong arrivals are evident to 7 km to the southwest (Fig. 4E); the first arrivals at 9 and 10 km are either delayed or attenuated, and arrivals are weak at greater distances. To the northeast, all first arrivals are weak. Arrivals are discernible, though weak, to about 13 km to the east but are weak toward the west (Fig. 4F). Thus, the refracted waves from SP5 generally have high attenuation except within 10 km to the southwest. SP5 is located where the seismicity changes character; to the northeast the seismic trend is narrow, whereas to the southwest it is more dispersed. The strong arrivals to the southwest indicate that there is structural complexity around SP5, but generally the relation between high seismic-wave attenuation and the seismic zone is supported by the observations at SP5.

A similar relation between attenuation of seismic waves and the seismic zone is present on the profiles from SP3 (not shown), which is near the northern part of the seismic zone. Also, the profiles from SP4, which is near the southeast margin of the rift (Fig. 1) where there is minor seismicity (Fig. 3) (*17*), show strong attenuation across the rift margin. This attenuation may be associated with the rift-bounding fault zone. A seismic-reflection profile and magnetic survey in the same area (*23*) indicate that this fault zone is 5 to 6 km wide and has about 1 km of throw down to the northeast. Other refraction profiles generally do not exhibit the high attenuation; for example, all arrivals on profiles from SP9, which is located outside the rift (Fig. 1), are strong, and the profiles from SP2 and SP8, which are located near the northwest margin of the Mississippi embayment (Fig. 1), are generally strong.

The data suggest that the high attenuation of refracted upper crustal seismic waves is associated with the axial seismic zone and the fault zone along the rift's southeast edge. Apparently, the strong attenuation across the axial seismic zone is in the Blytheville arch but not across the whole arch (only across active fault zones in the arch). Two fundamental causes of high attenuation are (i) defocusing of seismic energy by changes in velocity structure (for example, by a low-velocity layer) and (ii) seismic scattering and absorption.

High attenuation caused by defocusing is certainly a factor in the NMSZ because low-

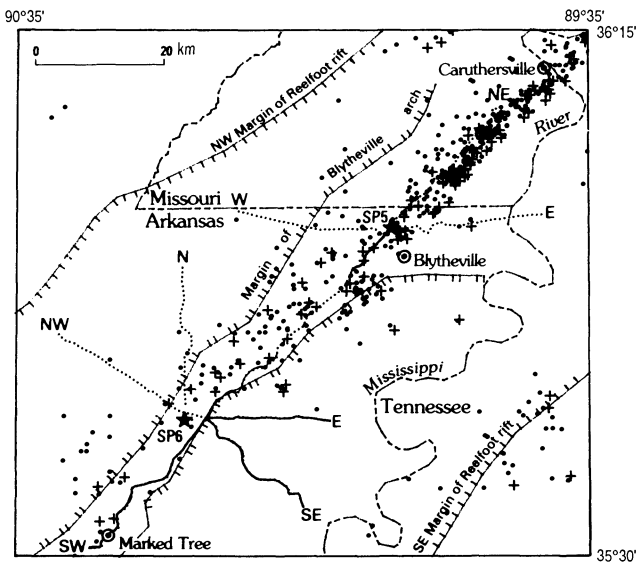

Fig. 3. Detailed map of the SP5 and SP6 area (shot points at stars). Profile lines are dotted where seismic waves are weak and solid where seismic waves are strong. Epicenters include a selected relocated set (pluses) (*15*) and the complete set (large dots) (*31*).

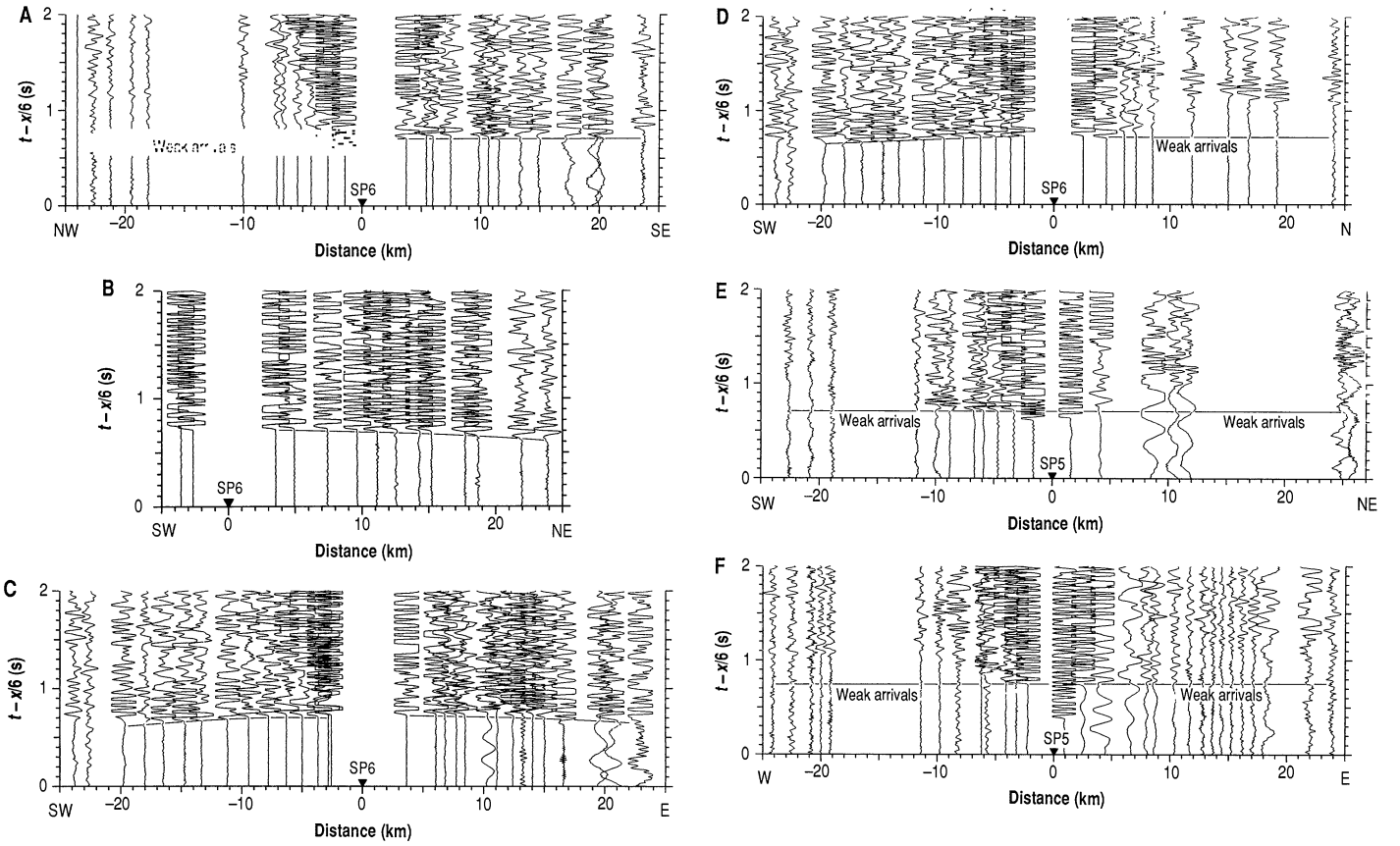

Fig. 4. Seismic-refraction profiles. (**A**) SP6 southeast-northwest profiles. (**B**) SP6 northeast-southwest profile. (**C**) SP6 southwest-east profiles. (**D**) SP6 southwest-north profiles. (**E**) SP5 southwest-northeast profiles. (**F**) SP5 east-west profiles. These seismic-refraction profiles demonstrate the large variability in seismic-wave attenuation, which apparently is associated with the seismic zone. All profiles are true-amplitude plots and have travel times (t) reduced to 6 km/s, where x is distance from the source.

velocity layers are known to be present in the subsurface. Sonic logs from the Dow Chemical #1 Wilson drill hole, which is located outside the Blytheville arch (Fig. 1), show average seismic-wave velocities of about 6.1 km/s for Knox-Arbuckle carbonates, 5.5 km/s for Elvins shale, 6.7 km/s for Bonneterre dolomite, and 6.1 km/s for basal sandstone; the underlying crystalline rocks have a velocity of 6.2 km/s or more. Thus, outside the arch, the Elvins and basal clastic units are relatively low-velocity strata interbedded with high-velocity units. The Elvins and basal clastic units thicken to over 7 km in the middle of the rift where they are structurally high because of the arch (Fig. 2). Moreover, sonic logs from the Dow Chemical #1 Garrigan drill hole, which is located on the arch where the Knox-Arbuckle carbonates are absent and in the seismic trend (Fig. 1), indicate that the velocities are substantially lower there: Elvins shale, 4.9 km/s; Bonneterre Formation, 5.5 km/s; and basal clastics, 4.9 km/s. Thus, the high attenuation could result not only from the structure of the Blytheville arch and the deep basin under it but also from anomalously low velocities of the rock units in the arch, particularly in the parts of the arch that have active fault zones. These low-velocity rocks, which deepen and are overlain by higher velocity carbonate rocks outside the arch, could form an effective seismic wave guide for propagation away from the arch. Such a wave guide would be manifested by abruptly attenuated seismic amplitudes for propagation away from the arch, as documented here.

Rocks in the fault zones associated with the Blytheville and the Pascola arches are probably extensively deformed because of the repeated episodes of tectonism that have affected the Reelfoot rift. Seismic-wave velocities of fault zones composed of fractured rocks are significantly reduced (*24*); thus, a low-velocity zone should be present under the arch. Such a zone could cause defocusing and high seismic scattering and absorption. The seismic arrivals that have wavelengths of about 600 m require 17 wavelengths to traverse the 10-km-wide arch; substantial attenuation through seismic scattering and absorption could occur over this distance but probably could not account for abrupt changes in wave amplitude. High seismic absorption has also been found at seismogenic depths in the San Andreas fault zone at Parkfield, California (*25*). High-attenuation zones delineated by seismic coda waves have been found to correlate with tectonically active areas (*26, 27*) and have been interpreted to measure fracture density (*28*). Other evidence for anomalously low seismic-wave velocities in the NMSZ zone comes from inversion of seismic-wave travel times (*29, 30*). These results, which apply mainly to the area of the Pascola arch (Fig. 1), suggest that average upper crustal seismic-wave velocities across the seismic zone are about 5.8 km/s as compared with 6.0 to 6.2 km/s in the surrounding area; the anomaly is attributed to high fluid pressures in the fault zone.

The strong attenuation of seismic waves by fault zones in the NMSZ may be a useful criterion for evaluating earthquake hazards, particularly for intraplate earthquakes. Zones of crustal weakness that are favorably oriented for slip with respect to the regional stress field generally are considered to be potential seismic source zones (*1*), but few of these zones are actually seismically active. Perhaps strong seismic-wave attenuation indicates particularly weak fault zones in the crust and therefore may be used to identify the zones that are prone to generating earthquakes.

REFERENCES AND NOTES

1. M. D. Zoback and M. L. Zoback, *Science* **213**, 96 (1981).
2. O. W. Nuttli, *Bull. Seismol. Soc. Am.* **63**, 227 (1973).
3. C. P. Ervin and L. D. McGinnis, *Geol. Soc. Am. Bull.* **86**, 1287 (1975).
4. M. F. Kane *et al.*, *Geology* **9**, 563 (1981).
5. T. G. Hildenbrand, M. F. Kane, W. Stauder, *U.S. Geol. Surv. Misc. Field Stud. Map MF-914* (1977).
6. T. G. Hildenbrand, *J. Geophys. Res.* **90**, 12607 (1985).
7. T. C. Buschbach and H. R. Schwalb, *U.S. Geol. Surv. Open-File Rep. 84-770* (1984), p. 64.
8. F. A. McKeown and R. M. Hamilton, *Geol. Soc. Am. Abstr. Programs* **99**, 99 (1989).
9. M. D. Zoback *et al.*, *Science* **209**, 971 (1980).
10. R. M. Hamilton and M. D. Zoback, *U.S. Geol. Surv. Prof. Pap. 1236* (1982), p. 55.
11. J. R. Howe and T. L. Thompson, *Oil Gas J.* (12 November 1984), p. 179.
12. A. J. Crone *et al.*, *Geology* **13**, 547 (1985).
13. R. M. Hamilton and F. A. McKeown, *Seismol. Res. Lett.* **59**, 117 (1988).
14. J. G. Grohskopf, *Subsurface Geology of the Mississippi Embayment of Southeast Missouri* (Missouri Geological Survey and Water Resources Report 37, Second Series, Rolla, 1955).
15. M. C. Andrews, W. D. Mooney, R. P. Meyer, *J. Geophys. Res.* **90**, 10223 (1985).
16. L. D. Himes, thesis, St. Louis University (1987).
17. W. Stauder, M. Kramer, G. Fischer, S. Schaefer, S. T. Morrissey, *Bull. Seismol. Soc. Am.* **66**, 1953 (1976).
18. R. B. Herrmann and J. Canas, *ibid.* **68**, 1095 (1978).
19. C. Nicholson, thesis, St. Louis, University (1980).
20. ———, D. W. Simpson, S. Singh, J. E. Zollweg, *J. Geophys. Res.* **89**, 4545 (1984).
21. W. D. Mooney, M. C. Andrews, A. Ginsburg, D. A. Peters, R. M. Hamilton, *Tectonophysics* **94**, 327 (1983).
22. A. Ginzburg, W. D. Mooney, A. W. Walter, W. J. Lutter, J. H. Healy, *Am. Assoc. Pet. Geol. Bull.* **67**, 2031 (1983).
23. T. G. Hildenbrand, *Geology* **10**, 476 (1982).
24. W. D. Mooney and A. Ginsburg, *Pure Appl. Geophys.* **124**, 141 (1986).
25. S. Blakeslee and P. Malin, *Eos* **69**, 1318 (1988).
26. S. Singh and R. B. Herrmann, *J. Geophys. Res.* **88**, 527 (1983).
27. A. Jin and K. Aki, *Bull. Seismol. Soc. Am.* **78**, 741 (1988).
28. ———, *J. Geophys. Res.* **94**, 14041 (1989).
29. H. J. Al-Shukri and B. J. Mitchell, *ibid.* **92**, 6377 (1987).
30. ———, *Bull. Seismol. Soc. Am.* **78**, 1491 (1988).
31. W. Stauder, R. Herrmann, S. Michell, M. Wuenscher, M. Whittington, *Central Mississippi Valley Earthquake Bull. 59* (St. Louis University, St. Louis, 1989).
32. We thank A. J. Crone, A. D. Frankel, C. Nicholson, F. A. McKeown, and L. C. Pakiser for helpful discussions and reviews of the manuscript and M. C. Andrews and R. B. Herrmann for copies of hypocenter files.

30 November 1989; accepted 23 February 1990

Theory of Spontaneous Vesicle Formation in Surfactant Mixtures

S. A. SAFRAN, P. PINCUS, DAVID ANDELMAN

The curvature elastic energy of bilayer vesicles formed by a mixture of two surfactants, which individually form either micelles or lamellar bilayer phases is described theoretically. In the limit of large bending elastic modulus K being much greater than the temperature T, the free energy is minimized by vesicles with different concentrations of the two surfactants in each monolayer of the bilayer. Vesicles are more stable than lamellar structures only when interactions or complexing of the two surfactants is taken into account.

RECENT EXPERIMENTS (*1*) PROVIDE strong evidence for the spontaneous formation of an equilibrium phase of large single bilayer vesicles from mixtures of two ionic surfactants with oppositely charged head groups. Indeed, most previous observations of thermodynamically stable vesicles also involved surfactant mixtures (*2–4*) or systems with mixed counterions (*5*). We present a continuum, theoretical model based on curvature energy concepts (*6*) for the equilibrium formation of vesicles with a preferred radius in mixed surfactant systems. Within this model, we find that vesicle formation requires nonideal mixing of the surfactants within a membrane and that it only occurs in the presence of complexing interactions.

Previous theoretical models that predict equilibrium vesicles (as opposed to lamellar or micellar phases) even for single surfactants have focused on the case of either small vescicles (*7*), or on the case of surfactant bilayers with small (compared to temperature T) curvature elastic modulus (*6*) K; the vesicles are then stabilized by entropic effects (*7–9*). In our model, which focuses on the limit of large K (>0), the most probable state for the pure surfactant solutions is either small micelles or lamellar bilayer phases. However, when the two surfactants are mixed, a vesicular phase can be stabilized by the curvature energy; the vesicles are stable (with respect to the lamellar phase) even in the limit of large curvature elastic modulus. The vesicular phase has lower free energy than the lamellar phase (*10*) because the mixing—when complexing or nonideality is included—allows the formation of surfactant bilayers where the two monolayers have different surfactant concentrations, which may result in equal and opposite monolayer spontaneous curvatures (*6*).

We consider the free energy of a phase composed of a dilute solution of monodisperse, spherical vesicles where surfactants labeled "1" and "2" are mixed in a single solvent. Since our goal is to demonstrate the stabilization of the vesicles by their "internal" free energy, we consider the case where the translational entropy as well as interactions between the layers can be neglected (*10*). The vesicle is composed of inner and outer monolayers with curvatures (*11*) $\pm c$ to lowest order in the ratio of the surfactant thickness δ to the vesicle radius $R = 1/c$. In general, each monolayer has a different composition, and we denote the spontaneous curvatures (*6*) of the inner and outer monolayers by c_i and c_o, respectively. The spontaneous curvature of films formed by pure surfactants "1" and "2" are c_1 and c_2, respectively. The curvature elastic energy (*12*) of the vesicle per unit area f_c is given (*6*) by

$$f_c = 2K[(c + c_o)^2 + (c - c_i)^2] \qquad (1)$$

For simplicity, we have assumed that the bending modulus K of the mixed system is independent of the composition. In the case of the pure surfactants, the curvature energy is minimized by the formation of micelles [when c_1 and c_2 are consistent with the packing constraints (*13*)] or lamellar bilayers [when c_1 and $c_2 << \delta^{-1}$, with δ a molecular size].

The physical origin of the spontaneous curvature of a monolayer is the asymmetry in the packing densities of the polar and nonpolar regions of the amphiphile (*13, 14*). If we assume, for simplicity, that the hydrophobic regions of the two surfactants are identical but that their polar groups are different, the composition dependence of c_o and c_i arises from the composition dependence of the bond distances in the polar parts of each monolayer. Let ψ_i and ψ_o be the molar fraction of surfactant "2" in the inner and outer monolayers, respectively; the molar fraction of surfactant "1" is then $1 - \psi_i$ or $1 - \psi_o$, respectively. A random-mixing (*15*) approximation for the average distance a_i between polar heads in the inner layers yields:

$$a_i = a_1(1 - \psi_i)^2 + a_2\psi_i^2 + (1 - \gamma)(a_1 + a_2)\psi_i(1 - \psi_i) \qquad (2)$$

S. A. Safran, Exxon Research and Engineering, Annandale, NJ 08801.
P. Pincus, Materials Department, University of California, Santa Barbara, CA 93106.
D. Andelman, School of Physics and Astronomy, Tel Aviv Univ., Ramat Aviv, 69978 Israel.